AD-A113 831 NAVAL POSTGRADUATE SCHOOL MONTEREY CA F/G 11/3
A STUDY OF THE BREAKDOWN MECHANISM OF AISI 304 STAINLESS STEEL,--ETC(U)
DEC 81 M H BEELBY, H G ULRICH

UNCLASSIFIED NL

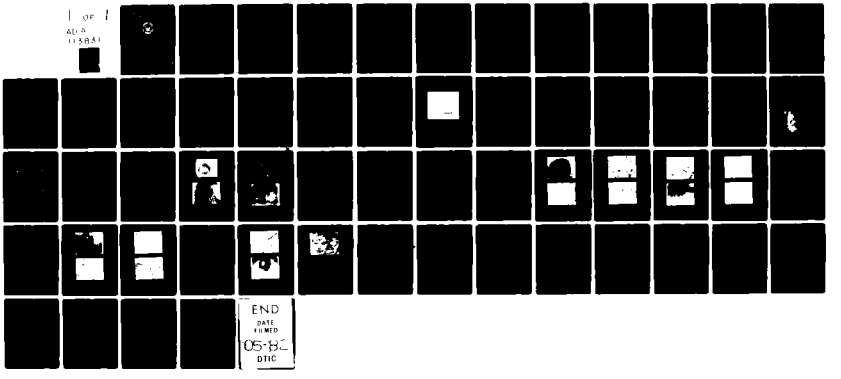

END
DATE FILMED
05-82
DTIC

NAVAL POSTGRADUATE SCHOOL
Monterey, California

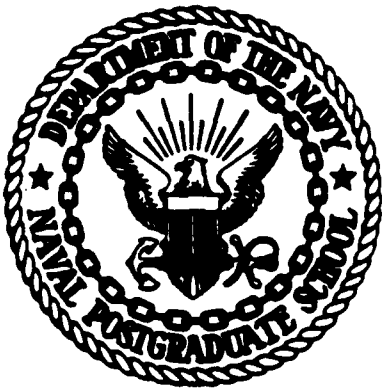

THESIS

A STUDY OF THE BREAKDOWN MECHANISM OF AISI 304 STAINLESS STEEL, TYPE 2024 ALUMINUM AND VARIOUS TITANIUM COATINGS

by

Michael Howard Beelby

and

Henry George Ulrich III

December 1981

Thesis Advisor: F. Schwirzke

Approved for public release; distribution unlimited

UNCLASSIFIED

SECURITY CLASSIFICATION OF THIS PAGE (When Data Entered)

REPORT DOCUMENTATION PAGE	READ INSTRUCTIONS BEFORE COMPLETING FORM
1. REPORT NUMBER	2. GOVT ACCESSION NO. AD-A113831	3. RECIPIENT'S CATALOG NUMBER
4. TITLE (and Subtitle) A Study of the Breakdown Mechanism of AISI 304 Stainless Steel, Type 2024 Aluminum and Various Titanium Coatings	5. TYPE OF REPORT & PERIOD COVERED Master's Thesis December 1981
	6. PERFORMING ORG. REPORT NUMBER
7. AUTHOR(s) Michael Howard Beelby Henry George Ulrich III	8. CONTRACT OR GRANT NUMBER(s)
9. PERFORMING ORGANIZATION NAME AND ADDRESS Naval Postgraduate School Monterey, California 93940	10. PROGRAM ELEMENT, PROJECT, TASK AREA & WORK UNIT NUMBERS
11. CONTROLLING OFFICE NAME AND ADDRESS Naval Postgraduate School Monterey, California 93940	12. REPORT DATE December 1981
	13. NUMBER OF PAGES 57
14. MONITORING AGENCY NAME & ADDRESS(if different from Controlling Office) Naval Postgraduate School Monterey, California 93940	15. SECURITY CLASS. (of this report) Unclassified
	15a. DECLASSIFICATION/DOWNGRADING SCHEDULE

16. DISTRIBUTION STATEMENT (of this Report)

Approved for public release; distribution unlimited

17. DISTRIBUTION STATEMENT (of the abstract entered in Block 20, if different from Report)

18. SUPPLEMENTARY NOTES

19. KEY WORDS (Continue on reverse side if necessary and identify by block number)

Unipolar Arcing
Plasma Surface Interaction
Titanium Coatings

20. ABSTRACT (Continue on reverse side if necessary and identify by block number)

An investigation, experimental and theoretical, into the breakdown mechanisms and associated minimum power levels required for the breakdown and unipolar arcing was conducted for AISI 304 stainless steel and Type 2024 aluminum. The experiment was conducted using a neodymium-glass Q-switched laser. A system of filters was used to attenuate the irradiance on target to the point at which no damage was discernible following laser-target interaction.

(continued)

DD FORM 1 JAN 73 1473 EDITION OF 1 NOV 65 IS OBSOLETE
S/N 0102-014-6601

UNCLASSIFIED
SECURITY CLASSIFICATION OF THIS PAGE (When Data Entered)

Item 20. (Contd)

Experimental results show that above a certain critical power density, surface breakdown occurs. The primary mechanism of surface damage at the power density threshold is by unipolar arcing.

Titanium coated stainless steels were exposed to energy density levels on the order ot 5 GW/CM^2. The titanium coatings significantly reduced or eliminated the number of unipolar arcs observed.

A model is proposed for the physical processes involved in the first few nanoseconds before breakdown.

Approved for public release; distribution unlimited

A Study of the Breakdown Mechanism of AISI 304 Stainless Steel, Type 2024 Aluminum and Various Titanium Coatings

by

Michael Howard Beelby
Lieutenant Commander, United States Navy
B.S., United States Naval Academy, 1971

and

Henry George Ulrich III
Lieutenant Commander, United States Navy
B.S., United States Naval Academy, 1972

Submitted in partial fulfillment of the
requirements for the degree of

MASTER OF SCIENCE IN ENGINEERING SCIENCE
(Michael Howard Beelby)

MASTER OF SCIENCE IN PHYSICS
(Henry George Ulrich III)

from the

NAVAL POSTGRADUATE SCHOOL
December 1981

Author: _____

Author: _____

Approved by: _____ Thesis Advisor

_____ Second Reader

_____ Chairman, Department of Physics and Chemistry

_____ Dean of Science and Engineering

ABSTRACT

An investigation, experimental and theoretical, into the breakdown mechanisms and associated minimum power levels required for the breakdown and unipolar arcing was conducted for AISI 304 stainless steel and Type 2024 aluminum. The experiment was conducted using a neodymium-glass Q-switched laser. A system of filters was used to attenuate the irradiance on target to the point at which no damage was discernible following laser-target interaction.

Experimental results show that above a certain critical power density, surface breakdown occurs. The primary mechanism of surface damage at the power density threshold is by unipolar arcing.

Titanium coated stainless steels were exposed to energy density levels on the order of 5 GW/CM^2. The titanium coatings significantly reduced or eliminated the number of unipolar arcs observed.

A model is proposed for the physical processes involved in the first few nanoseconds before breakdown.

TABLE OF CONTENTS

ACKNOWLEDGEMENT

We wish to thank Mr. Robert Sanders for his invaluable assistance. Without his help this project would never have gotten off the ground.

We would also like to acknowledge the inspiration, support and advice provided by Professors Schwirzke and Challenger. While they saved us from the frustrations of false starts they allowed us the freedom to make this a most rewarding and enjoyable academic experience.

Last, but by no means least, we are indebted (one of us eternally) to Mary Ulrich for her editing and clerical assistance. While we were able to find a threshold for surface breakdown, we never were able to find a threshold for her patience and understanding.

I. INTRODUCTION

The quest for fusion power has been hampered by many technical problems not the least of which has been surface wall erosion. A magnetically confined plasma required for nuclear fusion expands radially by diffusion and comes in contact with the surrounding solid walls of the vacuum chamber which provide an essential part of the plasma confinement. The resultant interaction of the plasma with the boundary is dominated by erosion processes. The erosion at the wall leads to the introduction of impurities into the plasma which limit the achievable plasma parameters. Furthermore, the erosion of the wall material has a deleterious effect on the material integrity. The different possible erosion processes are [1]:

- -sputtering by D, T, He, impurity ions and neutrons
- -arcing between the plasma and the solid wall (unipolar arcs)
- -heat pulses to the first wall which may cause localized evaporation and surface cracking
- -the gas implanted into the first wall can lead to chemical erosion, embrittlement and may cause blistering

Of these, unipolar arcing is now considered by some to be the dominant process. Efforts to date to limit plasma-surface erosion have had limited success. These efforts have included:

-optimum choice of wall material

-material coatings

-mechanical divertors

-material preparation schemes

Arcing across electrodes has plagued engineers since man harnessed electrical power. The literature is rich in studies of the arc mechanism. Yet, the discovery of the unipolar arc phenomenon is as recent as 1958 [2] and it is not yet fully understood. The aforementioned fusion energy application has provided the impetus for intense research into studying the arcing mechanism and damage kinetics. Other technologies will certainly benefit from this continuing research. Short pulse, high voltage plasma switches come immediately to mind. Shedd and Ryan in their work [3] also allude to the High Energy Laser and Particle Beam Weapon programs.

The previous theses research in this field at the Naval Postgraduate School has contributed to the development of the Schwirzke and Taylor Unipolar Arc Model. A Q-switched neodynium laser fired at a target surface has been used to produce a hot dense plasma to study the plasma/surface interaction. Unipolar arcing has been shown to be the primary damage mechanism when a plasma is formed in laser target interaction. Metal erosion by this process is much more severe than for homogeneous energy deposition. The implications for laser weapons are obvious. If the energy

density of the laser beam incident on a target exceeds that required for the creation of a plasma then subsequent laser energy will be attenuated by the heating of the plasma. This plasma in turn causes the unipolar arcs. The main thrust of our study seeks to determine how energy and momentum coupling to the target is influenced by unipolar arcing. Furthermore, in support of the Naval Postgraduate School's continuing search for arc resistant materials, a series of experiments were conducted on titanium coatings and the results are reported herein.

No further study into this material would be proper without first acknowledging the significant accomplishments of those who have previously labored in this field. For this and for the sake of completeness, an historical perspective is included herein, culminating in the current unipolar arc model as proposed by Schwirzke and Taylor [4].

II. HISTORY OF UNIPOLAR ARC PHENOMENON

A. ROBSON AND THONEMANN MODEL

The term unipolar arc was first coined by Robson and Thonemann in 1958. In their article concerning a metal plate exposed to a plasma, they theoretically derived the existence of an arc which "required only one electrode and is maintained by the thermal energy of the plasma electrons" [2]. Furthermore, they reported the results of two experiments which physically demonstrated this unipolar arc process on a mercury electrode. The basis of their model is that at equilibrium there must be zero net current between an exposed metal plate and a plasma. Considering the much higher velocity of the plasma electrons when compared to the ions, a retarding potential is established between plate and plasma. This floating sheath potential (V_f), as it is called, prevents all but the higher energy electrons in the maxwellian distribution to reach the wall. This negative potential also attracts the ions. Thus at equilibrium the net current becomes zero. The sheath potential was shown to be [2]

$$V_f = \frac{kT_e}{2e} \ln \frac{m_i}{2\pi m_e}$$

where: T_e = temperature of electrons

m_e = mass of electrons

m_i = mass of protons

e = electron charge

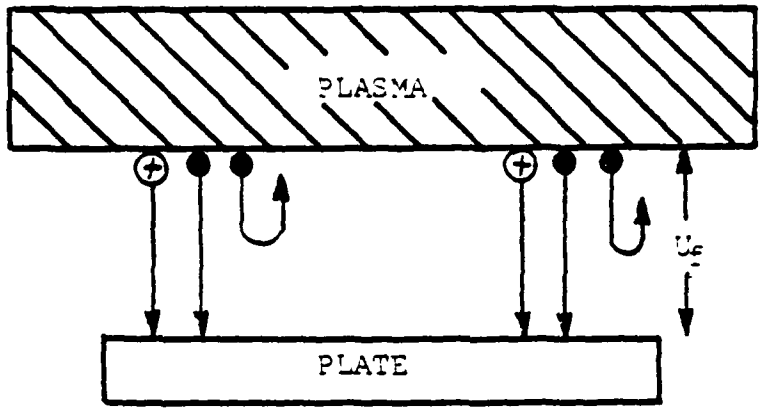

⊕ ION ● ELECTRON

Figure 1. Equilibrium of isolated plate with no cathode spot.

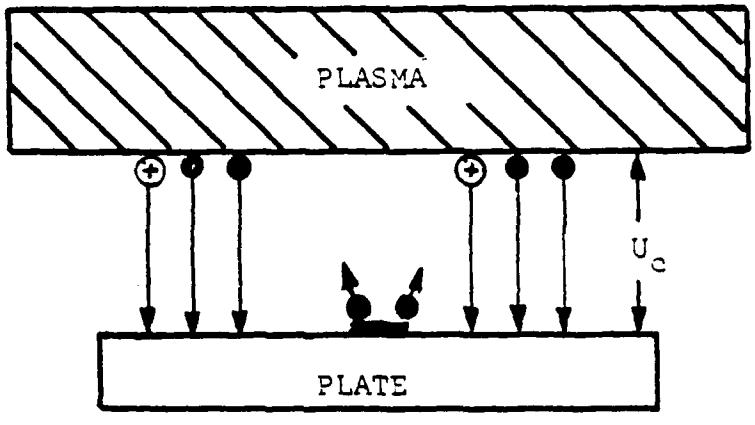

⊕ ION ● ELECTRON

Figure 2. Equilibrium of isolated plate with a cathode spot.

Figure 1 is a diagram of the Robson and Thonemann model at equilibrium.

If the electron temperature (T_e) is sufficiently large such that V_f exceeds the potential to initiate and sustain an arc, the authors now argued that there will be a strong local emission of electrons from the plate (cathode) to the plasma. The potential then lowers from V_f to V_c, where V_c is the cathode fall potential of the arc. With the voltage now lowered more electrons can return to the plate, thus closing the current loop and maintaining the plasma's quasineutrality. Figure 2 represents this process. The circulating current is given by [3]

$$I_c = An_e \left[\frac{(kT_e)}{(2\pi m_3)}\right]^{\frac{1}{2}} \left\{ \exp \frac{(-eV_c)}{(kT_e)} \quad -\exp \frac{(-eV_f)}{(kT_e)} \right\}$$

where: A = area of the plate exposed to the plasma

n_e = electron density of plasma

The arc was sustained, they now argued, until I_c fell below a minimum current I_a. The value of I_a depends on the material of the plate.

The existence of unipolar arcs has been verified with extensive experimental evidence.

B. SCHWIRZKE AND TAYLOR MODEL

This model was first presented in 1980 [4] and later elaborated upon by Ryan and Shedd [3]. Again as in the Robson and Thonemann model a sheath potential V_f is established between the plasma and surface material. For an arc to develop a locally enhanced electric field must exist.

$$E_{SHEATH} = \frac{V_f}{\lambda_d}$$

The Debye shielding length (λd) is given by

$$\lambda_d = (kT_e/4\pi n_e e^2)^{\frac{1}{2}}$$

Micro-protrusions on the surface material would cause this locally enhanced electric field. The ion flux would increase at these spots causing local heating, and in turn desorption of gases, vaporization and metal evaporation. Schwirzke and Taylor showed that a fraction of the neutrals thus emitted could be ionized in the sheath, thus effectively increasing the plasma density near the surface. Since $\lambda_d \alpha n_e^{-\frac{1}{2}}$ there is a narrowing of the sheath width and concomitantly an increase in the electric field strength. There will also be a local increase in the plasma pressure above this spot (now appropriately referred to as the cathode spot), and this results in a radial electric field (E_r) in the plasma. E_r is given by [4]

$$E_r = -(kT_e/e)\ (1/n_e)\ (dn_e/dr)$$

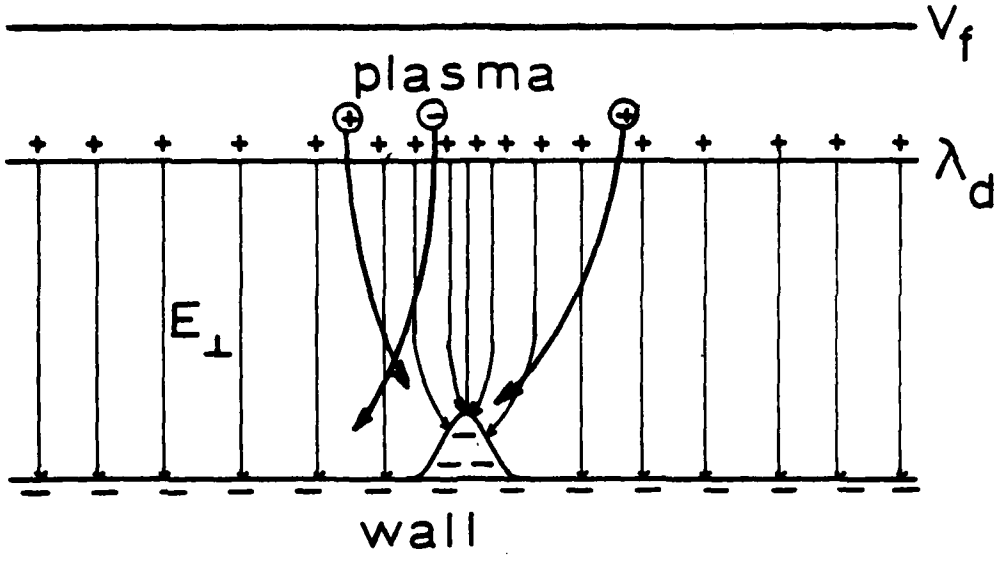

Figure 3. Field Enhancement at Surface Inhomogeneity.

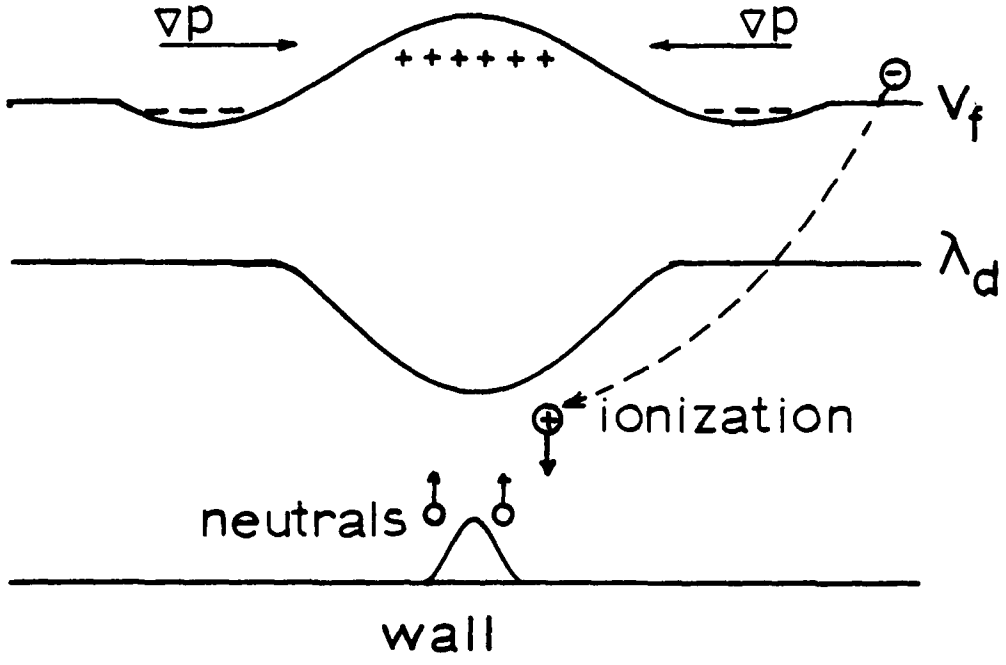

Figure 4. Increased Plasma Density over cathode spot due to ionization of evaporated neutrals produces narrower sheath width and increased ion bombardment and recombination at the cathode spot.

This radial Electric Field reduces the sheath potential in a ring like area surrounding the cathode spot. Thus a path of lower resistance is established for the electrons to return to the surface to close the current loop. Figure 3 and 4 illustrate the salient points of this process.

Referring again to the Robson and Thonemann equation for the circulating arc current where:

$$I_c = An_e (kT_e/2\pi m_e)^{\frac{1}{2}} \left\{ \exp(-eV_c/kT_e) - \exp(-eV_f/kT_e) \right\}$$

In their model they state that the area, A, is the whole of the surface area exposed to the plasma. Whereas the Schwirzke and Taylor model limits the area to the area of a ring surrounding the cathode spot over which the sheath potential is lowered.

III. EXPERIMENTAL APPARATUS

A system schematic of the experimental apparatus is included as Figure 5. A Bausch and Lomb and a Zeiss Optical Microscope together with a Cambridge Scanning Electron Microscope were used to inspect and categorize the target damage. A brief description of each piece of equipment is given below:

A. LASER SYSTEM

A Korad K-1500 Q switched neodymium glass laser was used to create the plasma on the target. Pulse energy varied between 6-13 joules. The 3db pulse width was consistently measured to be 20 msec. The laser pulse shape is shown in figure 6. The power irradiated on the target was controlled by introducing transmission filters. The laser energy output was measured using a Laser Precision RK-3230 meter inserted before the filter bank. Energy on the target was computed using the nominal transmittance of the filters and a combined 0.846 transmittance for the focusing lens and chamber window. The laser's beam size was measured by irradiating an exposed polaroid film. While this method did not provide for an energy distribution across the beam width it did provide a total beam width for determining the average power flux. The average power flux, $\bar{F}$ given in watts/cm^2 is thus:

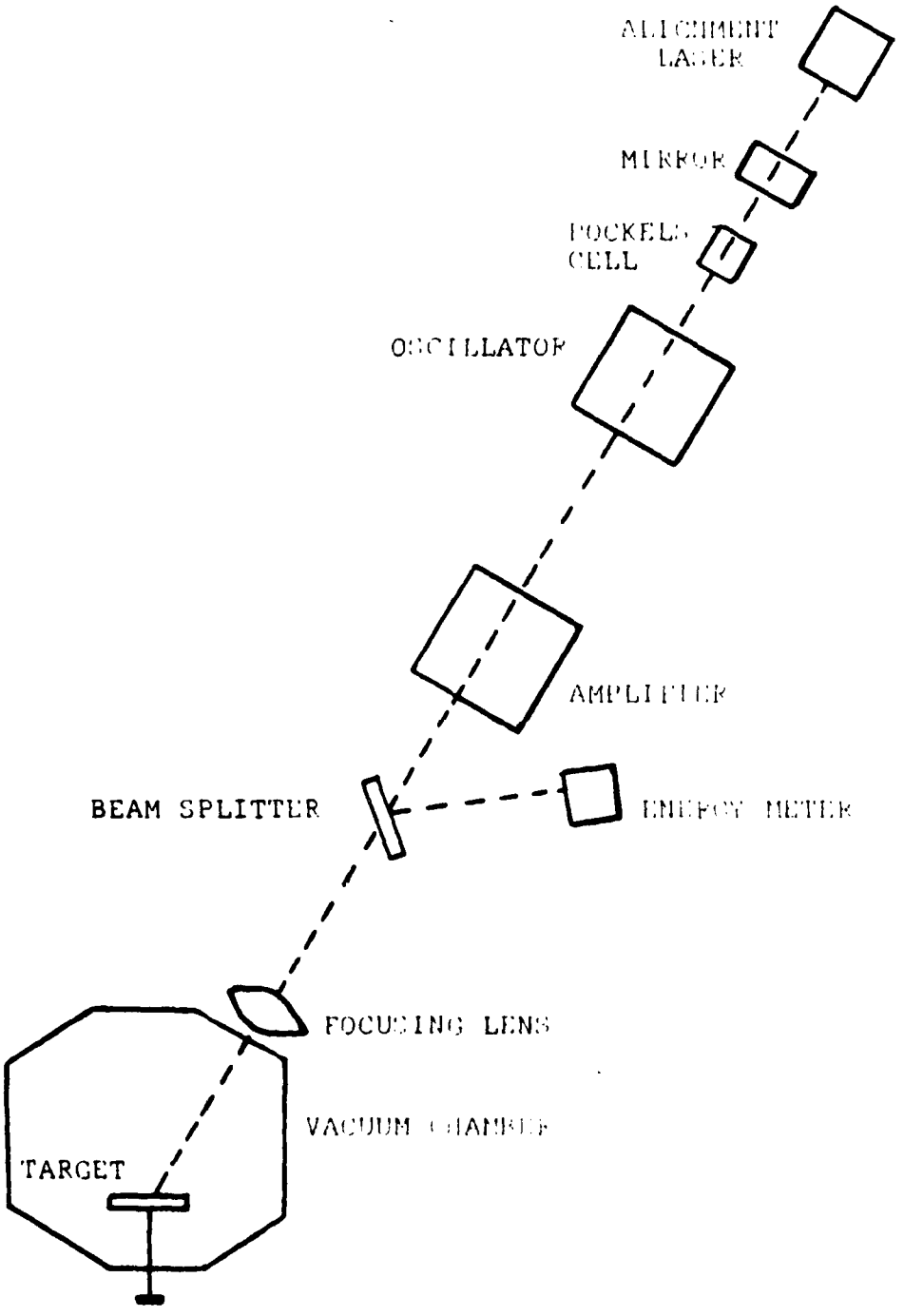

Figure 5. Laser and Test Chamber Arrangement.

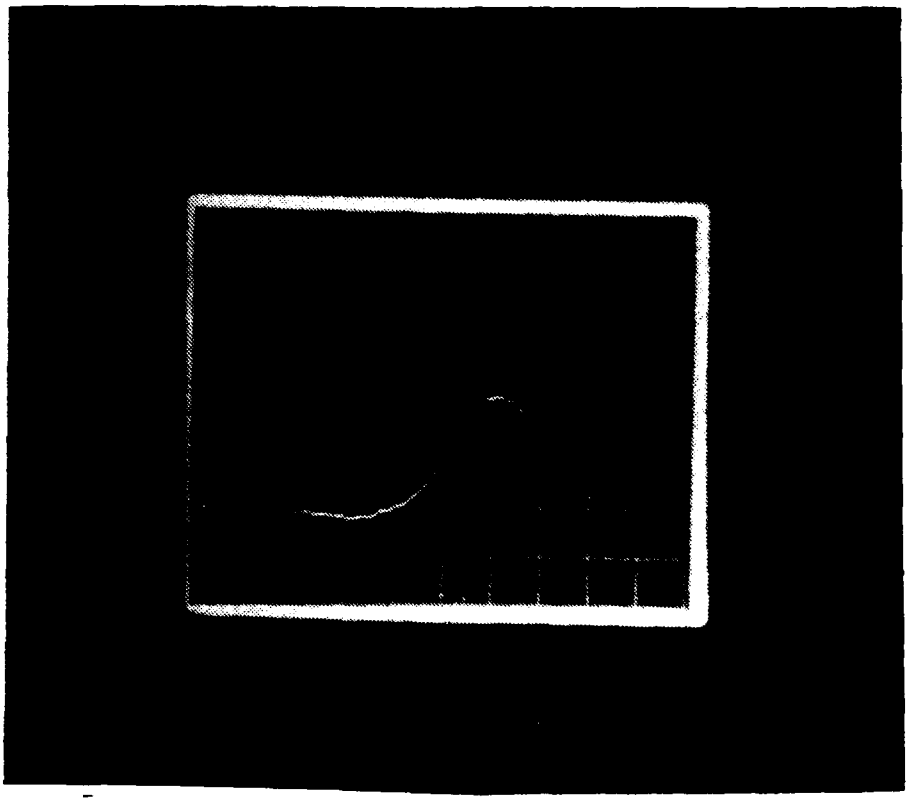

Figure 6. Laser Pulse Width

$$\bar{F} = \frac{ET}{\tau A}$$

where: E = energy (joules) measured by RK3230

T = Transmittance of optics and filter

τ = 3 db pulse width (secs)

A = beam area (cm^2)

More detailed information on the Korad K-1500 laser can be found in Davis' thesis [5].

B. ENERGY METER MODEL 3230

The Laser Precision Corporation's model 3230 energy meter consists of a pyroelectric detector and associated processing and display electronics. The meter will integrate the incident power signal over pulse durations of 1 nsec to 1 msec. The response of the detecting system is accurate to within $\pm$ 4%. The laser pulse passes through a beam splitter which is then filter attenuated prior to entering the energy meter to maintain the signal within the maximum sensitivity range of the instrument.

C. OSCILLOSCOPE

A Tektronix model 7104 oscilloscope was used to measure the incoming and reflected laser pulses. Incorporated in the oscilloscope were a model 7B10 time base and a model 7A24 dual trace amplifier. The time base allowed measurements to 2 nsec/div.

D. VACUUM CHAMBER

The target test chamber as shown in figure 5 is constructed of aluminum with an internal volume of 12.9 $\pm$ 0.3 liters. The chamber was designed and constructed by NPS personnel. The vacuum system, consisting of a mechanical pump and an oil diffusion pump with a liquid nitrogen cooled baffle, provided a chamber pressure down to 10^{-6} Torr. The laser beam was incident to the target at an angle of 30^{o}. A probe inserted in the rear of the chamber supported the target holder and allowed rotation of the holder. This arrangement allowed multiple targets to be exposed without the time consuming process of breaking and resetting the vacuum. A variety of other adapters were available for insertion of instruments.

E. SCANNING ELECTRON MICROSCOPE (SEM)

A Cambridge S4-10 Stereoscan SEM was utilized to conduct high resolution target surface inspections and damage assessment. The resolution in this equipment is at least 10 nm with a depth of focus of 300 times greater than that of an optical microscope.

The Stereoscan has a direct reading magnification system which provides a useful range between 20X and 100,000X corresponding to scanned areas of 5 mm to 2 microns square on the specimen.

The SEM was used in conjunction with a PGT 1000 XRAY microanalysis system.

F. SPECIMEN PREPARATION

Targets were mounted in bakelite and rough sanded. They were then polished (400 grit) using an AB Duo Belt Wet Sander, and hand polished using a 600 grit (wet) paper. Final polishing was accomplished using a 1 micron diamond paste. Final polishing using the non-aqueous diamond paste reduced the amount of pitting on the target surfaces. Specimens were cleaned using distilled water, acetone, and ethanol following the final polish. The specimens were then removed from the bakelite and ultrasonically cleaned in acetone. Finally the specimens were stored in a dessiccator until mounting for insertion in the target chamber.

IV. EXPERIMENTAL RESULTS

A. DETERMINATION OF POWER DENSITY THRESHOLD FOR ONSET OF ARCING

1. AISI 304 Stainless Steel

a. Description

The incident laser power density for the onset of arcing was determined for type 304 stainless steel by varying the laser energy incident on a target. The experimental set-up is as shown in Figure 5. The energy output is more easily controlled by the introduction of filters and changing the irradiated target area, than by adjusting laser power supply voltages. The incident power on the target was controlled in this manner.

The width and shape of the laser pulse were measured by the oscilloscope. The total energy in the laser pulse was read from the energy meter. After correcting for lens and filter attenuation, the power incident on the target could then be determined. A hand held polaroid camera was positioned above the target to note plasma formation by recording the attendant light. The beam spot size was measured by placing exposed polaroid film at the target position within the vacuum chamber and conducting a series of laser shots to find the average spot size area. The average power density, $\bar{F}$, is then:

$$\bar{F} = \frac{E}{A\tau}$$

where $\bar{E}$ = average incident energy

τ = 3 db pulse width, 20 nsec

A = exposed area

b. Results

Using this experimental arrangement a series of laser shots were made to determine the power density threshold for unipolar arc formation. Table I summarizes this series of experiments. Figures 7 and 8 provide a comparison of the extent of damage between target 3 (25.5 Mw/cm^2) and target 6a (5.4 Mw/cm^2). Figure 9 shows the characteristic hemispheric shape of the unipolar arc surrounded by a pronounced rim and the small dark cathode spot in the crater center.

A review of the target damage revealed that the damage was not evenly distributed across the laser spot size but was concentrated in one quadrant. By attenuating the energy incident on exposed polaroid film it was discovered that the energy in the laser beam was anything but uniform. The location of the beam's hot spot did however coincide exactly in shape and location with the previously reported target damage. Since the area used in calculating power density assumed a uniform distribution of energy, the threshold density reported herein can only be accurate as an order of magnitude power density for this particular laser. Further aggravating the overall accuracy of the reported results is the fact that the energy meter was before the filter bank

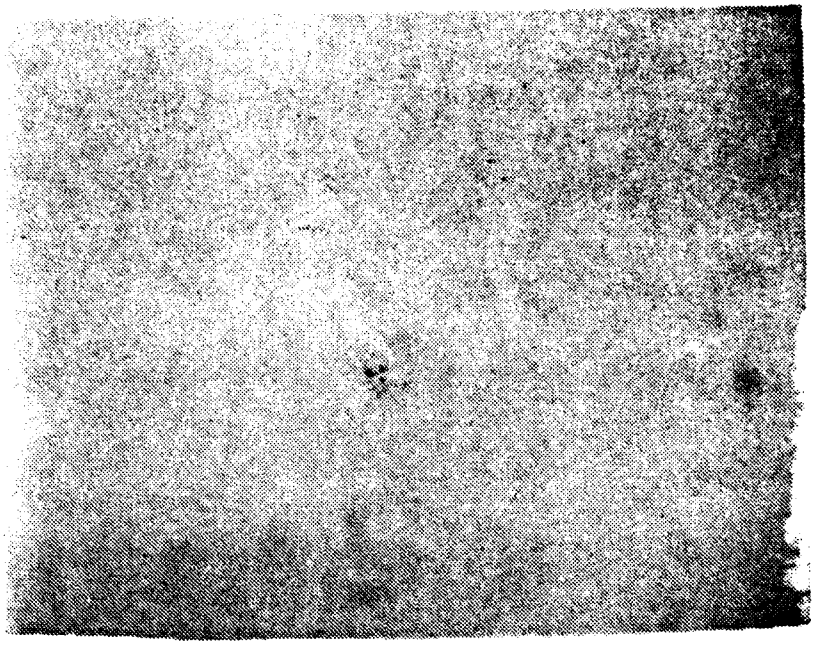

Figure 7. Target 6a, 5.4 Mw/cm^2
Target area magnified 100 X with SEM

Figure 8. Target 3, 25.5 Mw/cm^2
Target area magnified 100 X with SEM

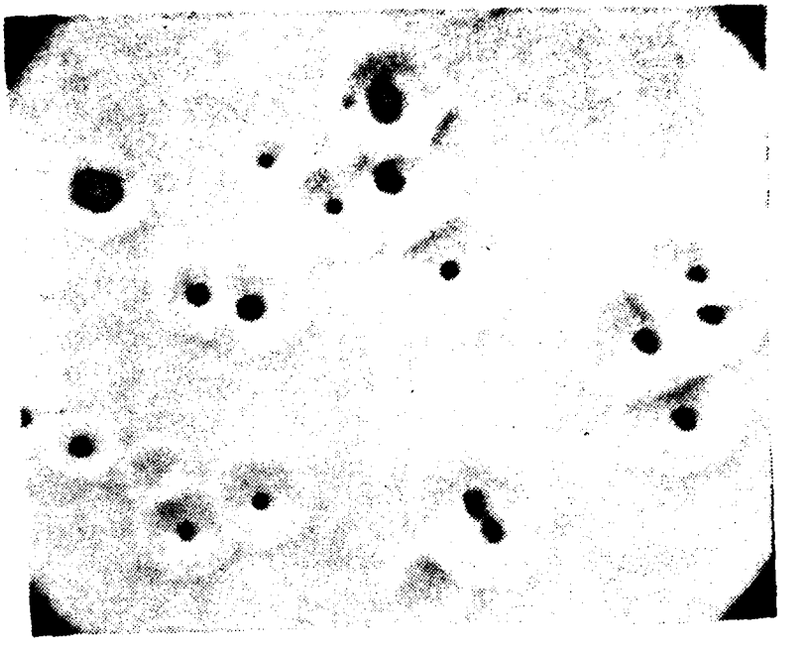

Figure 9. Target 6a, 5.4 Mw/cm
Target area magnified 2600 X with SEM

Table I: Summary of Results for Stainless Steel Type 304

Target Number	Power Density $\left(\frac{Mw}{cm^2}\right)$	Plasma Light	Arcing
1	23.1	*	Yes
2	64.4	*	Yes
3	25.5	Yes	Yes
4	13.3	Yes	Yes
** 6a	5.4	Yes	Yes
6b	5.1	No	No
7a	10.4	No	Yes
7b	13.6	Yes	Yes
8a	8.8	No	Yes
8b	8.2	No	Yes

* : Data not available.

** : Target 5 was used to compare beam area size. After target 5 two shots per target were utilized.

and in all calculations it was assumed that the filter attenuation was as reported on the nameplate data.

A further limitation in this series of tests was the limited sensitivity of the polaroid camera which served as a plasma recorder. In three of the tests the film did not show a plasma light yet one was certainly present since arc damage was in evidence.

c. Conclusions

The data thus obtained suggest that the power density threshold for the onset of breakdown and unipolar arcing in type 304 stainless steel is between an average power density of 5.1 and 5.4 Mw/cm^2. Hugill [6] theorized a power density for onset of arcing of 10 Mw/cm^2 for "steel". Further analysis of the data suggests that the onset of arc damage is coincident with onset of breakdown and plasma creation for stainless steel type 304. Never was there a plasma evident without attendant unipolar arcs. In fact at low power density there was no other direct laser damage like melting observed on the target. All damage was in the form of arc damage. The power density reported above is strongly dependent on an accurate measurement of the beam spot size and spatial distribution of energy. This is further discussed in Section VI.

2. Type 2024 Aluminum

a. Description

The incident power density for the onset of arcing for type 2024 Aluminum was determined in the same

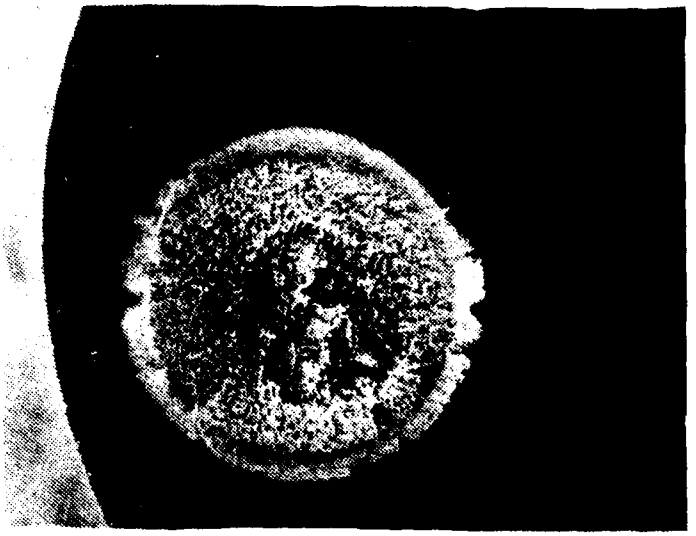

Figure 10. Aluminum target irradiated with 526 MW/cm^2. Laser impact area magnified 15 X with optical microscope.

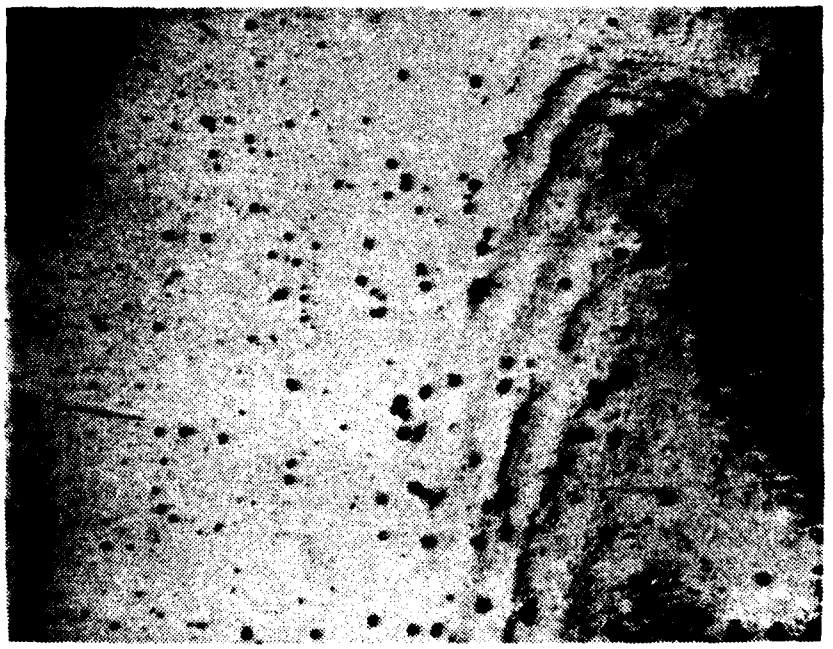

Figure 11. Aluminum target irradiated with 526 MW/cm^2. Just outside laser impact area magnified 100 X with optical microscope.

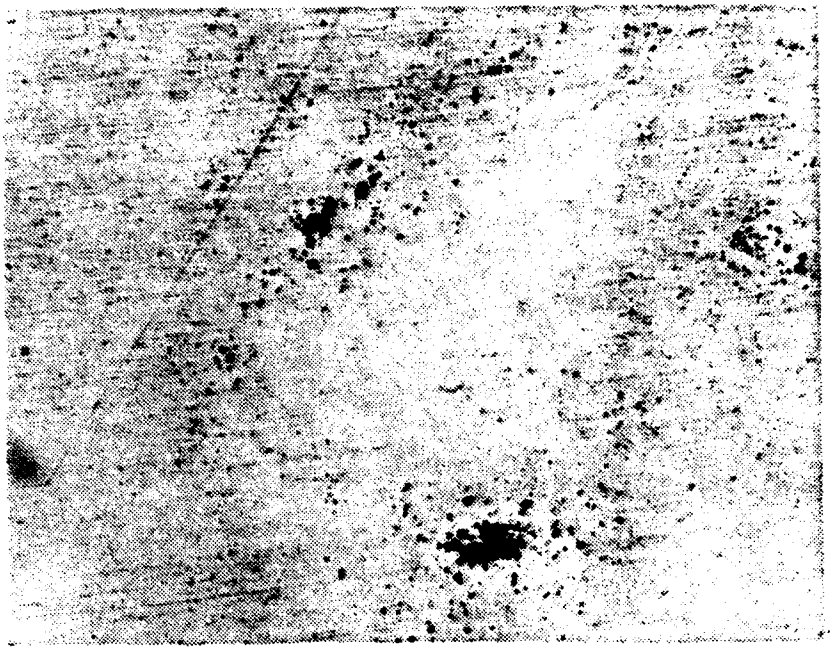

Figure 12. Aluminum target irradiated with 11 MW/cm^2. Laser impact area magnified 100 X with optical microscope.

Figure 13. Aluminum target irradiated with 20 MW/cm^2. Laser impact area magnified 240 X with optical microscope.

Table II: Summary of Results for Type 2024 Aluminum

Target Number	Power Density $\left(\frac{Mw}{cm^2}\right)$	Plasma Light	Arcing
1a	525.9	Yes	Yes
2	20.5	Yes	Yes
3	3.1	No	No
4	4.6	No	No
*1b	11.2	Yes	Yes

* There were two shots to different areas on target 1.

manner as for stainlesss steel. The experimental arrangement was modified only slightly by locating the power meter after the filter bank. This corrected for the previously mentioned uncertainty in the filter characteristics.

A wider aperture setting was used on the hand held polaroid camera which was then more sensitive in recording the light from the plasma.

b. Results

Table II summarizes the results for the series of experiments. After determining the onset of breakdown for aluminum was approximately 11.2 Mw/cm^2 a stainless steel target was exposed to the laser beam with the same degree of filtering. With an incident power of 10.9 Mw/cm^2 there was no evidence of plasma or arcing.

c. Conclusions

The results in table II suggest that the onset of breakdown and unipolar arcing for type 2024 aluminum is somewhere between 4.6 Mw/cm^2 (no plasma) and 11.2 Mw/cm^2 (plasma). Using this experimental set-up one target of type 304 stainless steel was irradiated with 10.9 Mw/cm^2 and neither a plasma nor arcs were evident. whereas in the previous section a threshold power density for this type of stainless steel was reported to be between 5.1 - 5.4 Mw/cm^2 The figures thus obtained had the power meter before the filters. Again, it should be noted that the figures reported herein assume a uniform power distribution across the laser beam when in reality this is not the case. Furthermore,

with the statistical variation that can be expected with this type of breakdown experiments the numbers reported should only be used as an order of magnitude power density for this particular laser.

Figure 10 shows the laser impact area for a high power shot of 526 Mw/cm^2 aluminum. At first glance it appears that the density of arc craters is substantially lower than for stainless steel. It should be noted, however, that the impact area is characterized by what appears to be resolidified splashes of molten aluminum. Since the time required for large scale melting, flowing and resolidification of the aluminum is presumably orders of magnitude larger than for the arcing process it is reasonable to assume that the arc craters were covered by the molten aluminum. Beyond the edges of the molten area the characteristic arc craters do appear (Figure 11). Figures 12 and 13 show the damage area and characteristic arcs at the onset of arcing at 11 and 20 Mw/cm^2. As in stainless steel never was there a plasma evident without attendant unipolar arcs.

B. STAINLESS STEEL WITH TITANIUM COATINGS

In addition to aforementioned investigations into the threshold of breakdown and arcing several experiments were conducted in support of the Naval Postgraduate School's continuing search for arc resistant materials - specifically three stainless steel samples which were coated with titanium

in different environments. The samples were obtained by Professor Schwirzke from "The Center for Plasma Physics and Fusion Engineering", U.C.L.A. The substrate is type 304 stainless steel. The coatings were applied by placing the substrate in a tokamak, called Macrotor, in the vicinity of a titanium bulb source. The titanium deposits on the substrate by sublimation. The titanium depositions were carried out at approximately 10^{-4} torr hydrogen pressure. The resulting coating is a titanium hydride (see section 2 below). After deposition, two samples were heated at a constant rate (40°C/mim) from room temperature to 700°C. One sample was outgassed in this manner in a vacuum (see section 3 below) while the other was accidentally outgassed in the presence of low pressure nitrogen probably forming titanium nitride (see section 1 below). All three samples were exposed to the focused unattenuated laser light intensity of approximately 500 Mw/cm^2.

1. Titanium on Stainless Steel Outgassed in Nitrogen

The resultant coating as explained above is a Titanium Nitride which had a shiny appearance. This unpolished sample was exposed to the focused laser beam with an incident energy of 5.4 joules. Figure 14 shows the laser impact area magnificed 22X by the Scanning Electron Microscope (SEM). The laser damage area averages 4 mm in diameter, Just right of center, the two darker elliptical areas are the only molten areas evident. These areas correspond to the

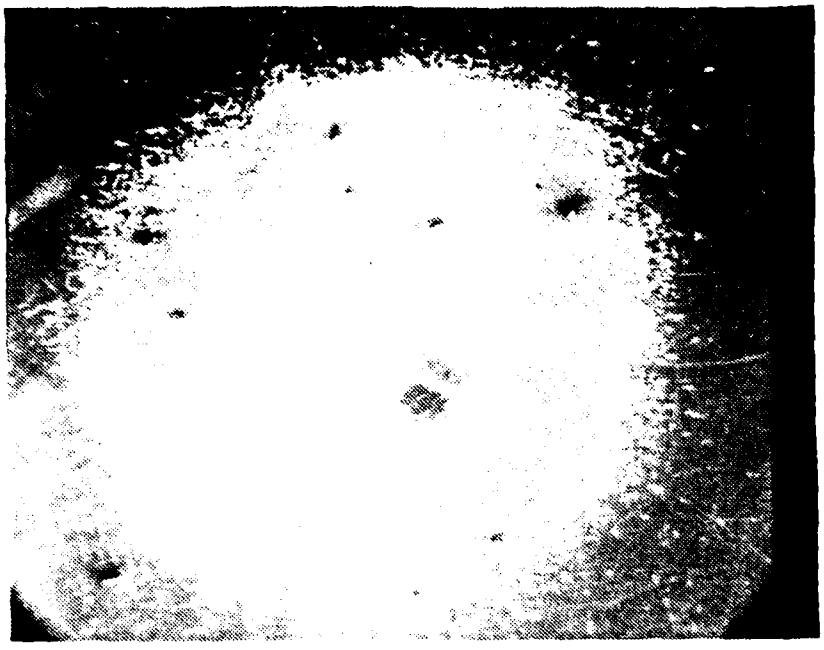

Figure 14. Ti on SS outgassed in nitrogen. Laser impact area magnified 22 X by SEM.

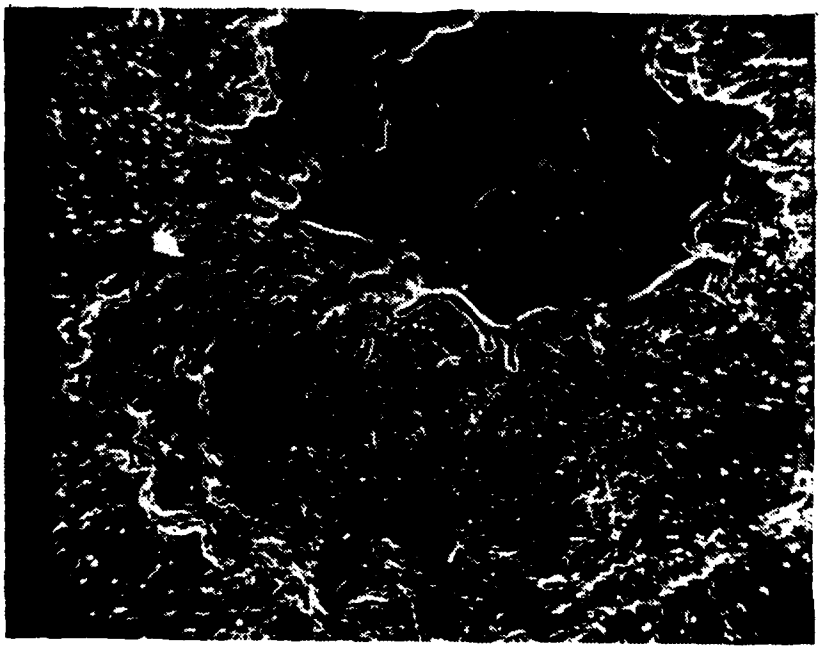

Figure 15. Ti on SS outgassed in nitrogen. Molten areas magnified 220 X by SEM.

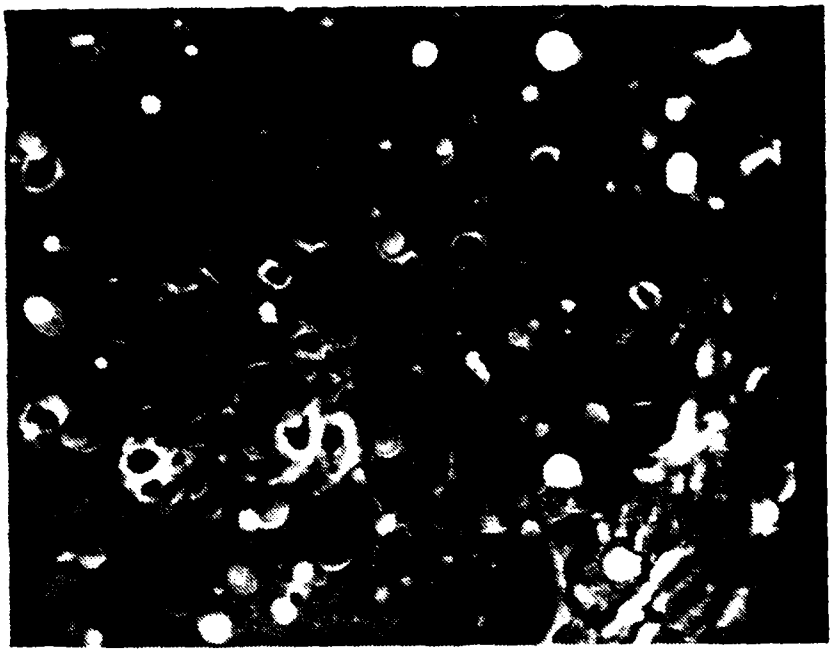

Figure 17. Ti on SS outgassed in nitrogen. Perimeter of molten area magnified 200 X by SEM.

Figure 1[illegible]. Ti on SS outgassed in nitrogen. Laser impact area magnified 2200 X by SEM.

Figure 18. Ti on SS outgassed in nitrogen. Laser impact area magnified 2200 X by SEM.

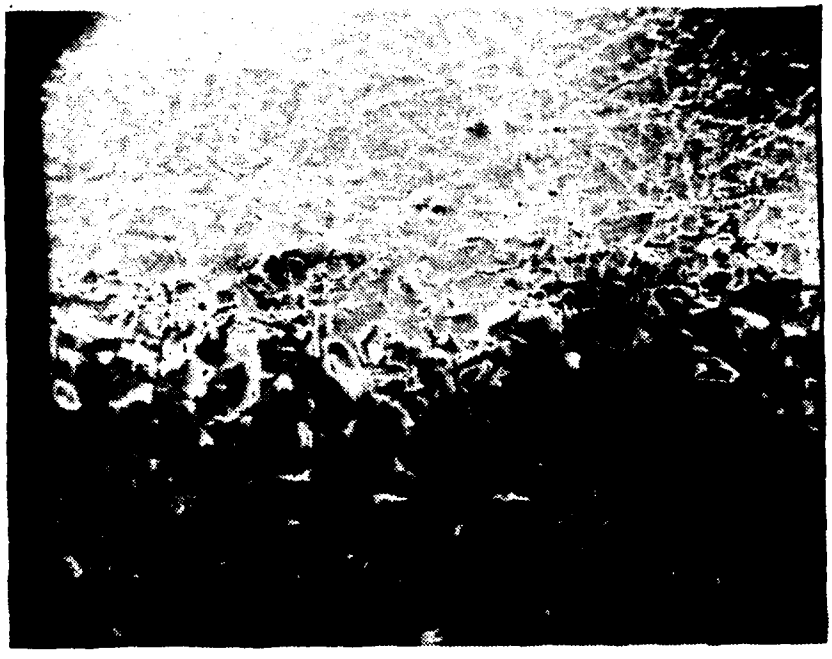

Figure 19. Ti on SS outgassed in nitrogen. Boundary between laser impact area and coating magnified 110 X by SEM.

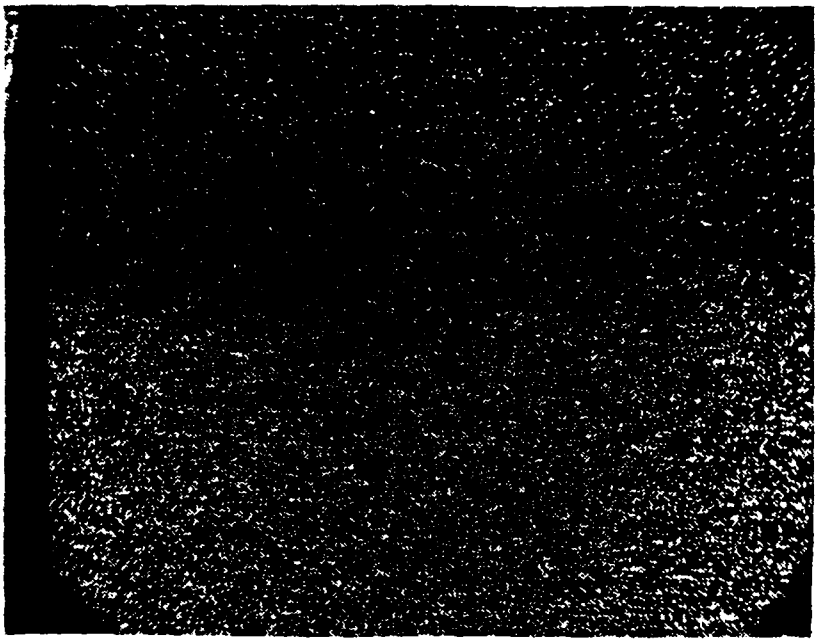

Figure 20. Ti on SS outgassed in nitrogen. Ti Xray map of boundary using SEM and PGT 1000. Same target area as Figure 20.

Figure 21. Ti on SS outgassed in nitrogen. Fe Xray map of boundary using SEM and PGT 1000. Same target area as Figure 20.

laser hot spot mentioned previously. They are magnified 220X in Figure 15. Post damage analysis of the target revealed unipolar arcs only on the perimeter of these molten areas. Figure 16 shows this region magnified 2200X. The diameter of the arcs are 1-2 microns. Figures 17 and 18 show typical areas also magnified 2200X in and around the laser impact area. Notice the absence of any unipolar arc craters.

Using the SEM an element map was made for both Ti and Fe. The area selected was the bottom of the laser impact area. As shown in Figure 19 the map area included the boundary between the laser impact area and the undamaged coating. The maps, Figures 20 and 21, dramatically show the density gradients of the two elements. The laser removed the titanium coating and exposed the stainless steel substrate. Yet, with the stainless steel thus exposed there are not any unipolar arcs in evidence as one might expect. The laser target interaction process in this case is unknown. As can be seen in the right side middle of Figure 19 it appears that the coating was torn away in relatively big chunks. The one in question is 45 microns long. We did not find any arc craters in the exposed substrate. In view of the relatively large mass involved, this is not suprising, since the time required to remove the coating was much greater than the laser pulse width and hence the plasma lifetime.

2. Titanium on Stainless Steel not Outgassed by Heating

This sample prepared as discussed above. The result is a coating of titanium hydride on a stainless steel substrate. The resultant coating is black in color.

This unpolished sample was exposed to the focused laser beam with an incident energy of 5.7 joules. Figure 22 shows the laser impact area magnified 22X by the SEM. A picture of the coating far removed from the impact area and thus unaffected by the laser is shown as Figure 23. This picture magnified 550X provides a contrast to the damaged coating area shown in Figure 24 at the same magnification. The surface roughness and cracks in the coating are similar in both pictures. The obvious difference in the damaged coating is the presence of microscopic holes in the coating. These holes are magnified to 2200X in Figure 25. These barnacle like disturbances in the coating are probably not unipolar arcs. However, having a diameter of 1 micron, they are about the same size as a unipolar arc cathode hole. They also do not have the characteristic cathode spot in the center of the crater or pronounced rims around the crater. Not being unipolar arcs, it is unknown what exactly they are but it is assumed some other corrosion process is at work here. Since this sample was not outgassed, it might be expanding cavities or blisters of trapped hydrogen due to the flash heating by the laser.

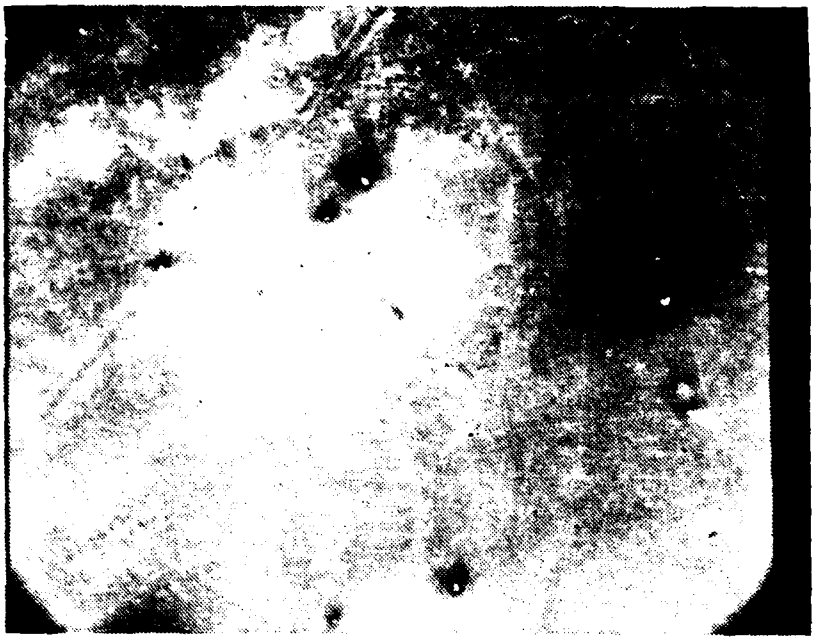

Figure 22. Ti on SS not heated. Laser impact area magnified 22 X by SEM.

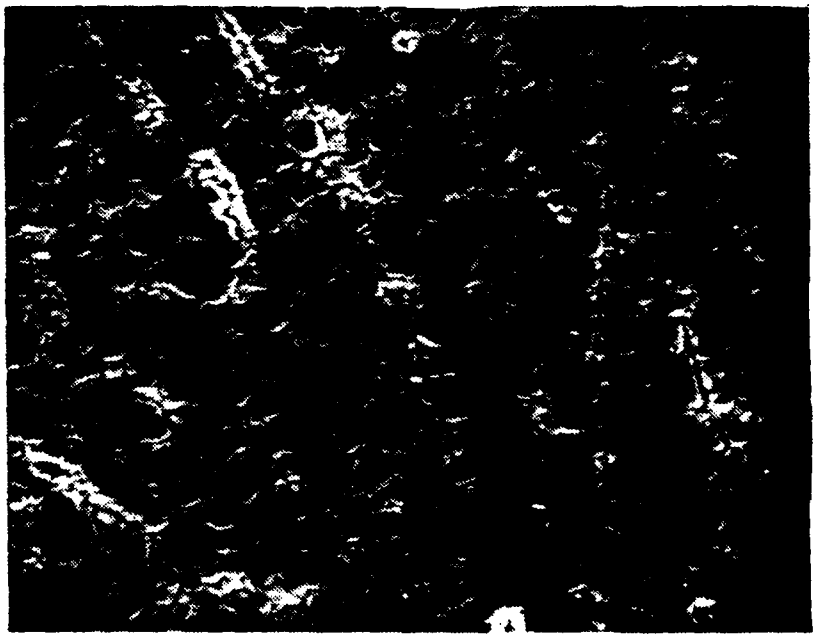

Figure 23. Ti on SS not heated. Undamaged coating magnified 550 X by SEM.

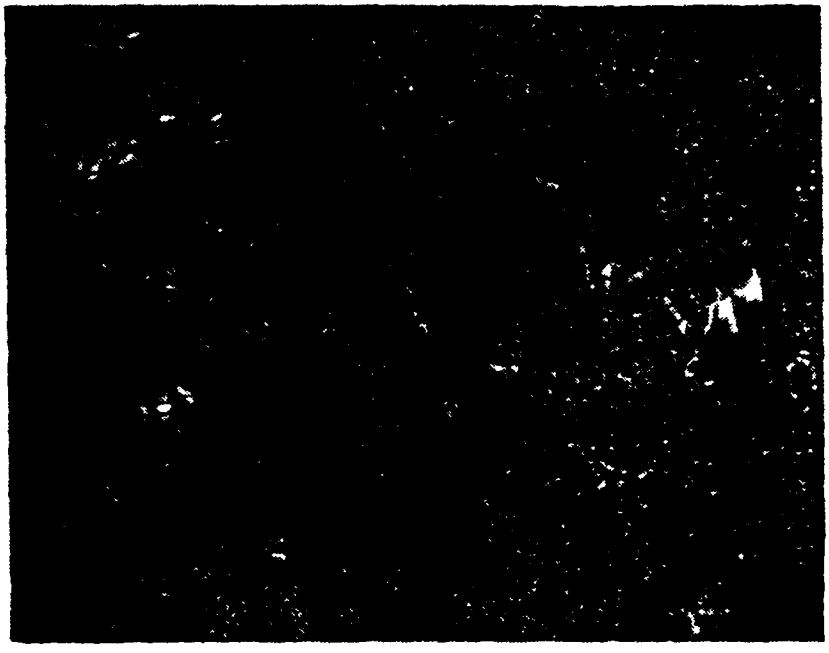

Figure 24. Ti on SS not heated. Laser impact area magnified 550 X by SEM.

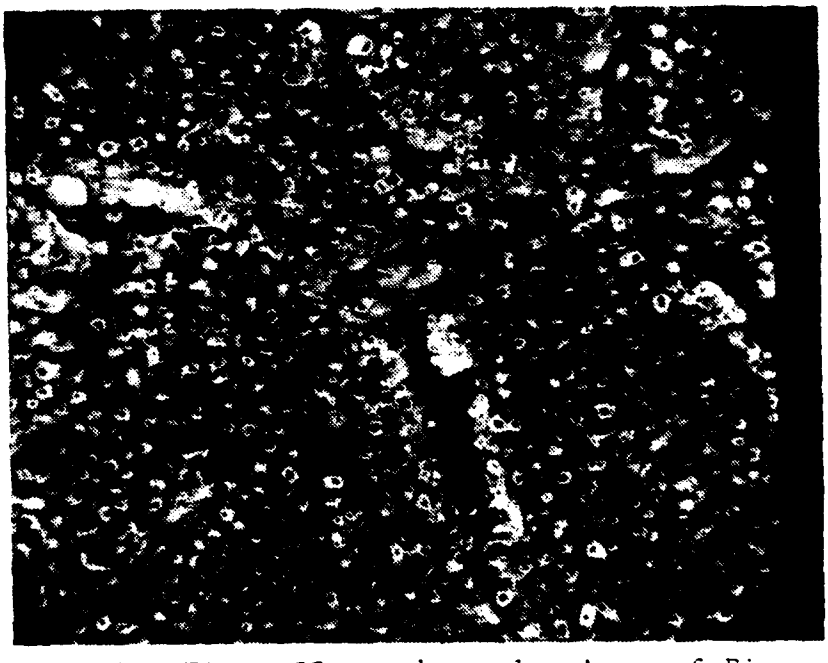

Figure 25. Ti on SS not heated. Area of Figure 24 magnified 2200 X by SEM.

3. Titanium on Stainless Steel Outgassed in Vacuum

This sample was prepared as was described above. The resultant coating was shiny in appearance. Its structure magnified 550X is shown as Figure 26.

This unpolished sample was exposed to the focused laser beam with an incident energy of 5.1 joules. Figure 27 shows the laser impact area magnified 22X. The dark area within the impact area was molten. The boundary between the laser impact area and the coating is shown in Figure 28. Again as in coatings not outgassed (section 2), the barnacle like structure appears. Again no unipolar arc craters were evident. The contrast in surface roughness between Figures 26 and 28 suggest that there was a smoothing process subsequent to irradiation by the laser.

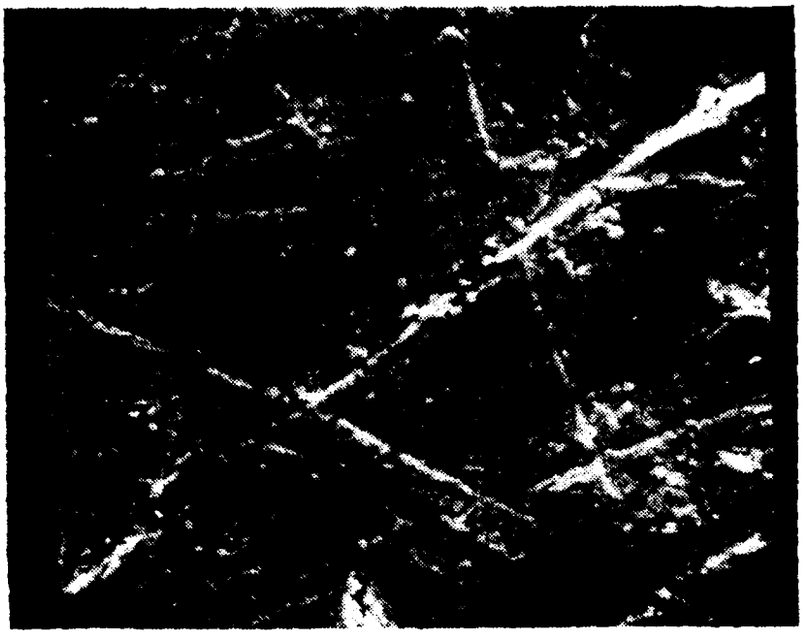

Figure 26. Ti on SS outgassed in vacuum. Undamaged coating magnified 550 X by SEM.

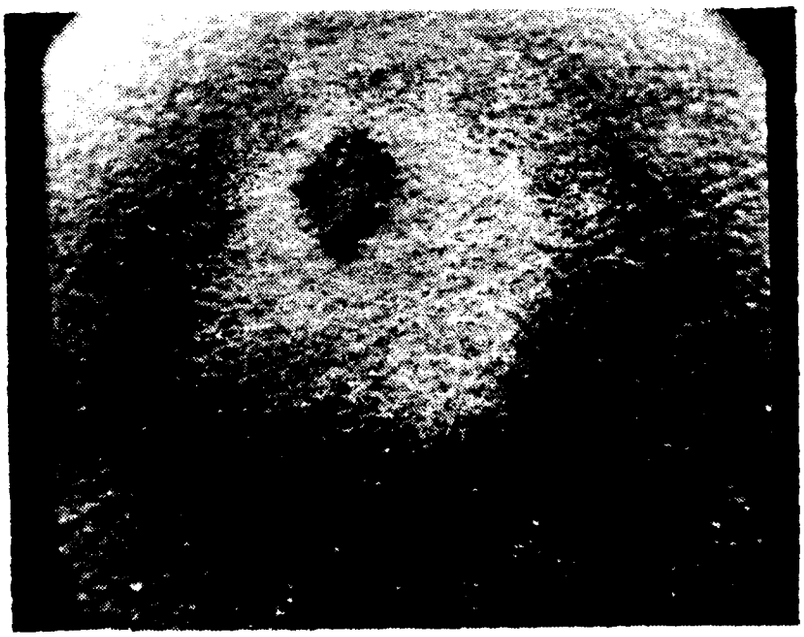

Figure 27. Ti on SS outgassed in vacuum. Laser impact area magnified 22 X by SEM.

Figure 28. Ti on SS outgassed in vacuum. Boundary area between laser impact area and coating magnified 500 X by SEM.

V. PROPOSED MODEL FOR THE ONSET OF SURFACE BREAKDOWN

Previous studies [3] have discussed the mechanisms which form the unipolar arc craters. In this study a model is proposed to explain what occurs prior to and during surface breakdown.

The experimental evidence reported in section IV suggests that at the threshold of surface breakdown for type 304 stainless steel and type 2024 aluminum there is no evidence of melting or ablation, the only damage evident is unipolar arcs. There was, therefore, a plasma in contact with the surface with the threshold plasma parameters necessary to cause arcing but no large area melting. It is assumed that that constituents of this plasma are ionized surface contaminants and that metal released from the arc cathode spots.

While great care was taken in the preparation and handling of the targets it is reasonable to assume that without extraordinary precautions, absorbed oxygen, water and oil are present on the surface of the target material prior to insertion in the test chamber. Furthermore, the vacuum in the chamber, being of the order of 10^{-6} Torr, was not high enough to remove all the surface contaminants. It is suggested that these contaminants are released and become ionized to form the seed plasma that causes onset of arcing.

The following assumptions are made in the development of this model:

(1) The surface of the target was prepared as discussed in section III. As such it is highly reflecting.

(2) Surface contaminants exist on the surface of the target. The main element is oxygen. The contaminants are closely packed with a monolayer surface density of typically 2×10^{15} atoms/cm^2. Only a monolayer is released for purposes of this discussion.

(3) The released gas is a perfect gas.

(4) The energy required to release the contaminants by desorption is negligible when compared to the ionization energy.

(5) A fully developed laser produced plasma is said to exist when the electron density, n_e, is greater or equal to the critical electron density for the Nd laser ($n_e \geq n_{ec} = 10^{21}$ cm^{-3}). The neutrals become slightly ionized.

(6) The characteristic time, τ , the laser pulse length is small and the flux is high so that plasma density losses such as via recombination and attachment can be ignored.

(7) Stray electrons are available and abundant to initiate plasma breakdown.

When the laser light first impacts the target surface most of the light is reflected. That which is absorbed

interacts with a volume defined by the laser spot size and skin depth (skin depth for type 304 stainless steel is estimated to be approximately 260 angstroms). This absorbed energy heats the thin surface layer and releases a monolayer of contaminants via thermal desorption. For our experimental spot size of 0.047 cm^2, this corresponds to a neutral number of atoms, N_0, of 10^{14} atoms. The minimum energy required to ionize these neutrals, assuming an average ionization energy of 32 eV per ionization for oxygen, is only E_i = 0.50 mJ (an accepted rule of thumb to allow for excitation and other energy loss mechanisms is to use an energy amount of 32 eV ionization for oxygen).

Nonetheless, it requires suprisingly little energy to create this seed plasma when compared to the total energy of 9.4 mJ reported in section IV to cause onset of surface breakdown. The plasma can thus be formed very easily early in the laser pulse. Using the approximately 8.9 mJ still remaining in the pulse after ionization to heat the plasma, and assuming an even distribution between ions and electrons, gives an electron temperature, T_e of 10^5 ^oK or 10 eV.

Assuming the plasma expansion rate is controlled by the ion expansion velocity which is equal to $V_i = (kT_e/M_i)^{\frac{1}{2}}$, this translates into 10^4 m/s. Using the laser pulse length, τ, as a characteristic time gives a characteristic expansion length of 100 microns and for an assumed even distribution of electrons a density of 10^{18} cm^{-3}. This in turn corresponds

to a characteristic pressue, p, of 25 atmospheres. In reality a density, temperature and pressure gradient exists with maximum pressure occurring near the critical density, n_{ec}.

When the monolayer of neutrals has been released, ionized, and heated to a sufficiently high T_e, the onset of arcing occurs on type 304 stainless steel in "vacuum". Below this power density of approximately 10 Mw/cm^2 surface damage to type 304 stainless steel is not evident. In view of the small amount of energy required to create the seed plasma, it is possible that for lower power densities a contaminant plasma can exist in contact with the surface with insufficient plasma temperature to cause arcing. However, there is no indication of this from our experimental results.

The assumption that little of the metal is in the plasma below these threshold power densities is supported by Ready [7]. He has computed the time for the metal to reach vaporization temperature at laser power densities of 10 Mw/cm^2 without breakdown for Fe and Al to be 0.186×10^{-6} sec and 0.267×10^{-6} sec respectively. Our laser pulse width is an order of magnitude shorter than this. Actually, once a plasma is formed most of the laser light is absorbed in the plasma and heats the plasma and little laser energy reaches the surface.

The plasma temperature derived above might suggest that the surface should melt as a fraction of the plasma energy reaches the target. It is assumed that this does not happen

due to the large heat conduction of the metal. If, however, the temperature continues to rise the target surface will reach the melting temperature and large scale melting and vaporization will occur. But prior to this, arcing already occurs locally with locally increased energy deposition on the surface, resulting in release of metal atoms from the cathode spot. This suggests very uneven energy deposition from the plasma to the surface as explained by the Schwirzke and Taylor Model discussed in section 2.

Assuming a highly polished target with relatively high reflectivity, it is reasonable to expect that a standing wave will set-up in the beginning of the laser pulse. For normal incidence the maximum electric field then would be located at $\lambda/4$ in front of the target and neglecting the skin depth the electric field will be zero at the surface. This electric field accelerates the stray background electrons which in turn ionize the released surface contaminants by collisional transfer of energy. As stated above the maximum electric field occurs at $\lambda/4$ and it is here, we assume, that most of the initial ionization occurs. In informal discussions with Naval Research Laboratory researchers it has been learned that they in fact have verified this phenomenon by using microwaves to create the plasma. By observing the light emitted they found that plasma creation does mainly occur at a distance $\lambda/4$ in front of the target. In view of the fact that for a neodynium laser $\lambda/4$ is 2.5×10^{-5} cm

no attempt was made to verify this observation using our experimental apparatus.

VI. CONCLUSIONS

Our experiments showed that for type 304 stainless steel and type 2024 aluminum the major damage mechanism in laser target interaction at the onset of surface breakdown is unipolar arcing. The power density for the onset of surface breakdown in "vacuum" for these materials is on the order of 10 MW/cm^2. This number is strongly dependent on the accurate determination of laser spot size and energy distribution. While not statistically significant it appears that type 2024 aluminum will breakdown with slightly less incident power than type 304 stainless steel. Since it is presumed that it takes the same amount of energy to create the seed plasma from the contaminants in both stainless steel and aluminum, this might suggest that the plasma threshold temperature required for arcing is less for aluminum than for stainless steel. A model has been developed to explain the processes at work in creating the correct conditions to cause surface breakdown.

For stainless steel with titanium coatings, prepared as discussed in section IV, and exposed to intense laser light, unipolar arcs did not contribute to the target damage. An exception was found in one sample which had the stainless steel substrate exposed during a portion of the laser pulse. Otherwise the major damage mechanisms were blow-off of the

coatings and an unknown corrosion process which formed a barnacle like structure on the exposed coating.

VII. RECOMMENDATIONS

If the model presented in section V is correct, it suggests that the cleaner the target the higher the power density required for onset of surface breakdown. By cleaner, we mean that the surface is free of surface contaminants and a seed plasma consisting of contaminants as described in section V can not be created easily at a distance of $\lambda/4$. This means that for surface breakdown to occur the metal itself must be vaporized. We maintain this will require more energy than desorbing surface contaminants.

It is suggested that a follow-on experiment be conducted to test this hypothesis. A vacuum chamber now exists in the plasma laboratory capable of maintaining 10^{-9} - 10^{-10} Torr. We expect that a target outgassed in this chamber and then irradiated by the laser will require a higher power density to cause surface breakdown than that required for targets prepared and irradiated as described in this paper. Furthermore, because of that higher power density one might expect that the target surface at the onset of breakdown will start to show evidence of ablation and melting.

As we noted previously the power density numbers reported herein are inversely proportional to the square of the laser spot radius. An accurate determination of a meaningful radius was troublesome throughout our experiments. A review

of the literature shows we are not alone in this concern. It is recommended that any further research projects that require an accurate measure of beam spot size start with the design of an accurate system to determine the spatial distribution of the laser energy.

The genesis of any research project starts with the search and accumulation of assorted reference material. After completing this phase of ours it was apparent that the significant time and effort exerted in this process simply duplicated those who preceeded us. Now that we have a dedicated laboratory in Spanagal Hall, it is recommended that a library be established there to collect all the pertinent references for this type of research. We have catalogued the references we used on 3 X 5 cards annotating the title, author, source and key points of the article. These will be placed in the Plasma Laboratory to start this program.

LIST OF REFERENCES

1. Behrisch, R., "Surface Erosion from Plasma Materials Interaction," Journal of Nuclear Materials, v. 85, 86, p. 1047-1061, 1979.

2. Robson, A. E., Thonemann, P. C., "An Arc Maintained on an Isolated Metal Plate Exposed to a Plasma," Institution of Electrical Engineers, v. 106, pt. A, supp. 2, p. 508-512, April 1959.

3. Ryan, R., Shedd, S., "A Study of the Unipolar Arcing Damage Mechanism on Selected Conductors and Semi-Conductors," M. S. Thesis, Naval Postgraduate School, Monterey, California, June 1981.

4. Schwirzke, F., Taylor, R. J., "Surface Damage by Sheath Effects and Unipolar Arcs," Journal of Nuclear Materials, v. 93, 94, p. 780-784, 1980.

5. Davis, L. J., "Self-Generated Magnetic Field Produced by Laser Bombardment of a Solid Target," M. S. Thesis, Naval Postgraduate School, Monterey, California, 1971.

6. Hugill, J., "An Arc-Resistant Target for the Divertor of a Fusion Reactor," Journal of Nuclear Materials, v. 87, p. 353-355, 1979.

7. Ready, J. F., "Effects of High Power Laser Radiation," p. 103, Academic Press, New York, 1971.

INITIAL DISTRIBUTION LIST

		Copies
1.	Defense Technical Information Center Cameron Station Alexandria, Virginia 22314	2
2.	Library, Code 0142 Naval Postgraduate School Monterey, California 93940	2
3.	Department Chairman, Code 61 Department of Physics and Chemistry Naval Postgraduate School Monterey, California 93940	1
4.	Assoc. Professor F. R. Schwirzke, Code 61Sw Department of Physics and Chemistry Naval Postgraduate School Monterey, California 93940	3
5.	Assoc. Professor K. D.Challenger, Code 69 Department of Mechanical Engineering Naval Postgraduate School Monterey, California 93940	1
6.	LCDR Henry G. Ulrich III 34 Cameron Road Huntingdon Valley, Pennsylvania 19006	2
7.	LCDR Michael H. Beelby 208 North Street Holly, Michigan 48442	2